

Review

Radar Observations of Liquid Water in the South Polar Region of Mars: Indications from Astrobiology Perspectives

Junyi Zhou ¹, Chunyu Ding ^{1,2,*} , Siting Xiong ³ , Yan Su ^{4,5}, Jiawei Li ^{6,7}, Mengna Chen ⁸ and Shun Dai ^{4,5} ¹ Institute for Advanced Study, Shenzhen University, Shenzhen 518060, China; 2020281095@email.szu.edu.cn² Tiandu-Shenzhen University Deep Space Exploration Joint Laboratory, Shenzhen 518060, China³ Guangdong Laboratory of Artificial Intelligence and Digital Economy (SZ), Shenzhen 518000, China; xiongsiting@gml.ac.cn⁴ Key Laboratory of Lunar and Deep Space Exploration, National Astronomical Observatories, Chinese Academy of Sciences, Beijing 100049, China; suyan@bao.ac.cn (Y.S.); dais@nao.cas.cn (S.D.)⁵ School of Astronomy and Space Science, University of Chinese Academy of Sciences, Beijing 100049, China⁶ Lunar Exploration and Space Engineering Center, China National Space Administration, Beijing 100086, China; lijawei1228_ty@163.com⁷ Deep Space Exploration Laboratory, Hefei 230026, China⁸ Hunan Institute of Technology, Hengyang 421002, China; 2014001896@hnit.edu.cn

* Correspondence: dingchunyu@szu.edu.cn

Abstract: In recent decades, extensive research has led to the understanding that Mars once hosted substantial liquid-water reserves. While the current Martian landscape boasts significant water-ice deposits at its North and South poles, the elusive presence of liquid-water bodies has remained undetected. A breakthrough occurred with the identification of radar-echo reflections at the base of the Martian South Pole, using MARSIS (Mars Advanced Radar for Subsurface and Ionospheric Sounding) in 2018. These radar echoes strongly suggest the presence of a highly concentrated liquid-water body. However, a counter-narrative has emerged, contending that the subterranean conditions beneath the ice cap, encompassing factors like temperature and pressure, may be inhospitable to liquid water. Consequently, alternative hypotheses posit that the observed bright echoes could be attributed to conductive minerals or water-absorbing clay-like materials. The ongoing discourse regarding the presence of liquid water beneath the southern polar ice cap is a hot topic in the realm of Martian exploration. The primary focus of this paper is to provide a comprehensive overview of Martian radar detection, the recent controversies regarding liquid water's existence in the Martian South Pole, and the implications regarding the potential existence of Martian life forms in the water on Mars. The revelation of liquid water on Mars fundamentally suggests an environment conducive to the viability of Martian life, consequently furnishing invaluable insights for future exploratory endeavors in the pursuit of Martian biospheres. In addition, this paper anticipates the forthcoming research dedicated to Martian liquid water and potential life forms, while also underscoring the profound significance of identifying liquid water on Mars in propelling the field of astrobiology forward.

Keywords: Mars; Martian orbiter-mounted radar; liquid water on Mars; life on Mars; Martian exploration



Citation: Zhou, J.; Ding, C.; Xiong, S.; Su, Y.; Li, J.; Chen, M.; Dai, S. Radar Observations of Liquid Water in the South Polar Region of Mars: Indications from Astrobiology Perspectives. *Universe* **2024**, *10*, 43. <https://doi.org/10.3390/universe10010043>

Academic Editor: Dirk Schulze-Makuch

Received: 9 November 2023

Revised: 1 January 2024

Accepted: 11 January 2024

Published: 16 January 2024



Copyright: © 2024 by the authors. Licensee MDPI, Basel, Switzerland. This article is an open access article distributed under the terms and conditions of the Creative Commons Attribution (CC BY) license (<https://creativecommons.org/licenses/by/4.0/>).

1. Introduction

The question of whether extraterrestrial life exists in the universe and whether other planets are suitable for human colonization has long been a primary focus of our space exploration [1,2]. The planet Mars, which is in the habitable zone of the solar system and is one of the closest planets to Earth, stands in contrast to Venus; therefore, it has attracted much attention and exploration as the most likely planet for future human colonization [3–5]. Its nature has sparked interest in the possibility of life's existence on Mars [6–8]. Human exploration of Mars through spacecraft missions started in the

1960s, with the hope of discovering extraterrestrial life on the planet [6,9–11]. Over the subsequent decades of research, it has been observed that the current surface conditions on Mars do not support the long-term existence of liquid water [12]. However, the Martian morphology shows that the presence of extensive networks of channels, outflow channels, dried-up deltas, and alluvial fan landforms suggests a history of abundant liquid water in Mars' past [12–14]. In the early 21st century, both Europe and the United States launched missions, such as the Mars Express and Mars Reconnaissance Orbiter, to explore the possibilities of life on Mars [15,16]. These missions carried radar instruments, such as MARSIS (Mars Advanced Radar for Subsurface and Ionospheric Sounding) and SHARAD (SHAlow RADar) that have extensively probed the Martian subsurface in the past decade, as shown in Figure 1a,b [17,18]. Those radars led to the discovery of significant water-ice deposits at the North and South Poles of Mars [19–22]. In 2020, China launched the Tianwen-1 mission to Mars, which also carried a radar payload on its orbiter, as shown in Figure 1c [23,24]. The name of the Chinese orbiter-mounted radar is MOSIR (Mars Orbiter Subsurface Investigation Radar). MOSIR is primarily aimed at probing the subsurface structure of Mars and finding water resources. Its detection frequency expands the frequency range of the other two radars [23,25].

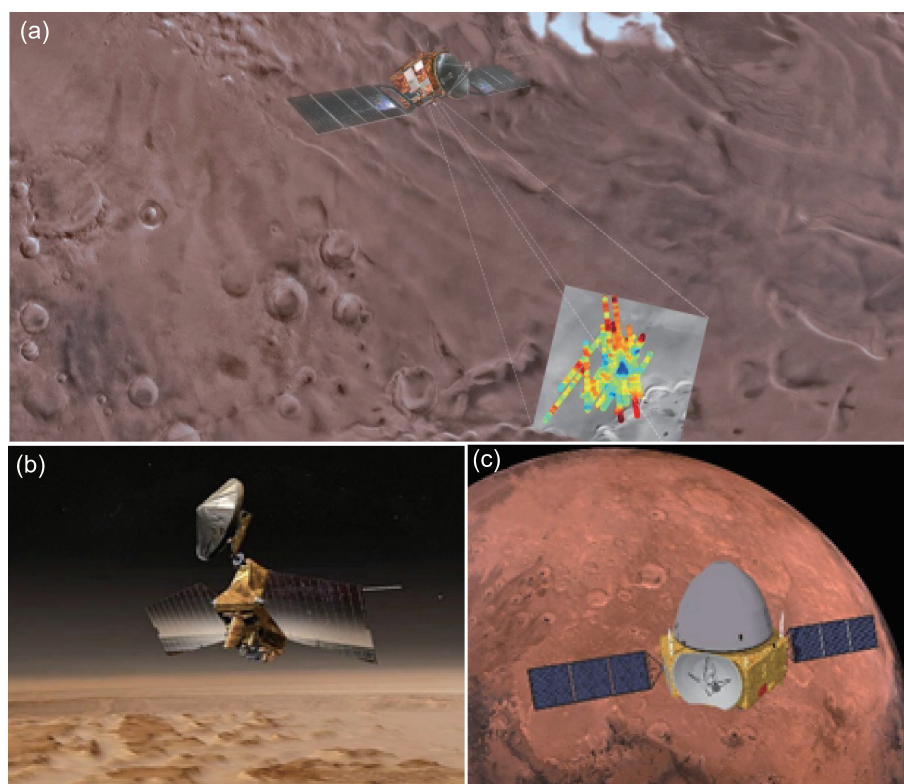


Figure 1. Radars carried by the three orbiters currently exploring Mars in orbit: (a) MARSIS radar onboard Mars Express mission; credit from the European Space Agency. (b) SHARAD radar onboard MRO mission [15]. (c) MOSIR radar onboard the Chinese Tianwen-1 mission; credit from the China National Space Administration (CNSA).

In recent years, MARSIS has identified bright reflections at the bottom of the Sub-surface Polar Layered Deposits (SPLDs) on the southern polar of Mars, and the detection principle is as shown in Figure 2. Orosei et al. [26] reasoned that these bright reflections are indicative of liquid water through the inversion of dielectric constants. They proposed that a high concentration of brines has lowered the freezing point of the liquid water, enabling its presence beneath the south polar ice cap [26]. Subsequently, Lauro et al. [27] discovered multiple bright reflections, using the latest MARSIS data, and suggested the existence of multiple liquid-water bodies at the bottom of the SPLDs. The presence of

liquid water implies the possibility of life on Mars and provides potential directions for human colonization. As a result, discussions regarding the existence of liquid water at the South Pole of Mars have ensued. Some researchers argue that even with high-concentration brines, the current temperatures and heat flux on Mars would prevent the existence of liquid water [28]. They suggest that the cause of the bright reflections might be differences in the dielectric properties of minerals at the bottom of the SPLDs [29] or clay [30]. Additionally, layered interference within the SPLDs has been proposed as one of the causes of the bright reflections [31]. In response to these doubts, researchers have conducted laboratory experiments to measure the dielectric properties of relevant materials under corresponding conditions. They argue that materials such as clay cannot cause such bright reflections and they continue to support the view that the cause of the bright reflections is brines with high chloride content [32,33]. Currently, the cause of these bright reflections remains inconclusive. The study of this area continues to be one of the hot topics in Martian exploration.

In this paper, we primarily provide an overview of the radar-based discovery of liquid water at the South Pole of Mars and its controversies. Meanwhile, we catch a glimpse of the significance of discovering water on Mars for the possibility of life on Mars. The main framework of the paper is as follows: First, we briefly introduce the operational principles of the Martian radar instruments, e.g., MARSIS, SHARAD, and MOSIR (see Section 2.2). Second, we discuss the permittivity inversion methods employed to inverse the liquid water on Mars, using MARSIS radar (see Section 3). Third, the recent debates concerning the existence of liquid water beneath the SPLDs ice layers are outlined in Section 4. Finally, we offer insights into the future exploration of liquid-water bodies on Mars and the potential search for Martian life (see Section 5).

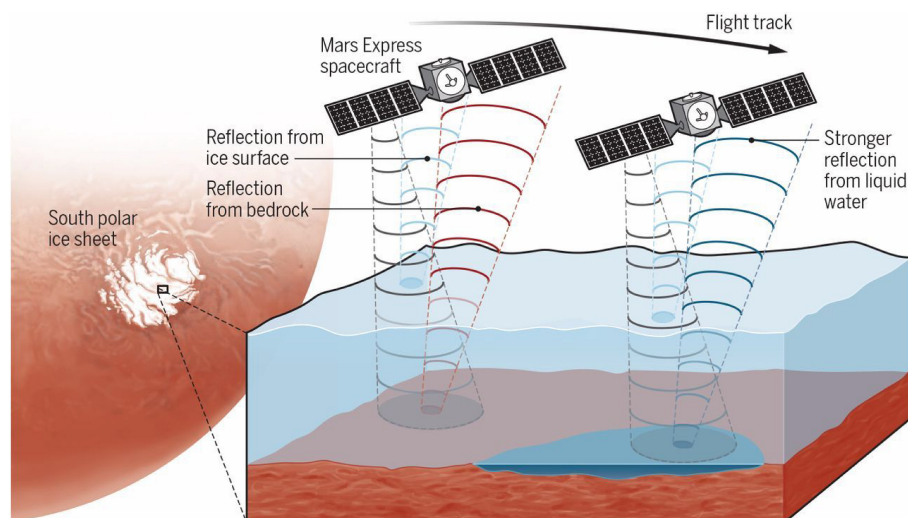


Figure 2. Schematic diagram of the Mars orbiter-mounted radar-detection principle. An example of MARSIS detecting liquid water under the Martian ice cap. Image source from the European Space Agency.

2. Detection Principles of Mars Orbital Radars

2.1. Introduction of Mars Orbital Radars

MARSIS is carried by the Mars Express spacecraft launched by the European Space Agency (ESA) (Figure 1a). It was initiated in August 2005 and is designed to explore the subsurface structures and ionosphere of Mars [34,35]. MARSIS consists of several components: (1) a 40 m-long dipole antenna oriented parallel to the Mars Express movement direction; (2) a 7 m-long monopole antenna perpendicular to the dipole antenna; (3) a dual-channel data processor; and (4) control units for power supply and electronic digital signals [36]. The primary antenna, the dipole antenna, is used to observe subsurface echoes from Mars. The secondary antenna, the monopole antenna, is employed to receive non-nadir reflections,

reducing interference with the echoes received by the primary antenna. When probing subsurface structures, MARSIS operates at four different frequencies: 1.8 MHz, 3 MHz, 4 MHz, and 5 MHz, each with a bandwidth of 1 MHz [37] (Table 1). The low-frequency pulses emitted by the radar enable the detection of structures several kilometers beneath the Martian surface [37].

Table 1. Basic parameters comparison of MARSIS, SHARAD, and MOSIR radars [23,37,38]

| Parameter | MARSIS | SHARAD | MOSIR |
|------------------------------------|------------------|--------|------------------------------|
| Operational frequency (MHz) | 1.8, 3, 4, and 5 | 15–25 | LF: 10–15/15–20 HF: 15–30 |
| Depth resolution in free space (m) | 150 | 15 | 30/7.5 |
| Designed penetrating depth (km) | 0.5–5 | 0.1–1 | 0.1–1 |

SHARAD is carried by NASA’s Mars Reconnaissance Orbiter, launched in August 2005 [39]. It primarily operates during the Martian night-time, to observe the subsurface structure and water ice on Mars [15]. SHARAD features a pair of 10 m-long dipole antennas and it operates at frequencies between 15–25 Hz [38,40]. Its high-frequency pulses provide a higher resolution than MARSIS, but its penetration depth is less than that of MARSIS. Table 1 provides a comparison of parameters between the two radars. Unlike MARSIS, SHARAD has a weaker surface-penetrating capability, due to its higher-frequency radar, which limits its ability to probe the subsurface hundreds–to–thousands of kilometers below the Martian surface. However, its high–resolution characteristics allow the radar to achieve more precise detection of the subsurface at depths ranging from tens to hundreds of meters on Mars. Consequently, SHARAD focuses on studying surface–related terrain structures and material composition [15]. MARSIS and SHARAD complement each other, in terms of exploration depth and radar resolution [41]. Over the past two decades, both radars have been utilized to survey Mars’ polar regions [42–44] and other areas [45–48], mapping terrain [43,49,50] and investigating the distribution of water ice on Mars [16,47,51,52]. In recent years, these radars have also hinted at the possible presence of liquid water on Mars [26], and they are further discussed in detail in Section 4.

In addition to the MARSIS and SHARAD radar systems, Mars also features the MOSIR radar onboard China’s Tianwen-1 mission, launched in 2020 (Figure 1c). MOSIR operates at three different frequencies: 10–15 MHz, 15–20 MHz, and 30–50 MHz, enabling penetration depths of several hundred meters into the Martian surface [23]. MOSIR emits either low- or high-frequency pulses, with vertical resolutions of 30 m and 7 m, and horizontal resolutions of several hundred meters (along-track) by several kilometers (cross-track) (see Table 1). Unlike the previous two radar systems mentioned, MOSIR radar employs two pairs of orthogonal dipole antennas (9 m in the cross-track direction and 10 m in the along-track direction). The antennas in the along-track transmit radar pulse and the whole cross-dipole antennas are utilized for echo reception. This configuration enables the reception of cross-track echoes, providing additional information for material-property analysis [23]. Apart from investigating Martian water ice, MOSIR is also designed to provide insights into aspects such as searching for potential life, surface terrain, and the internal structures of Mars [23,53,54].

2.2. Detection Principles of Mars Orbital Radars

The radars exploring Mars operate in different modes, including MARSIS’ SS1, SS2, SS3, SS4, SS5, and AIS (Atmospheric and Ionospheric Sounding mode). MARSIS uses the SS1–SS5 modes (subsurface sounding mode) while detecting the subsurface of Mars (such as liquid water under the Martian ice caps) and selects different modes according to the diversity of the topography [17]. Similarly, MOSIR has three operational modes: HFSS, LFSS plus ISS, and ADM [23]. The radars select the appropriate operational modes based on the specific exploration requirements. The spacecraft carry multiple operational modes,

and the radars generate substantial raw data, due to varying penetration depths and resolutions. The downlink of the data can potentially influence the radar operations. Therefore, the radars need to address issues related to onboard preprocessing, mode coordination, utilization of polarization information, compression ratios, etc. [55–59]. Furthermore, each operational mode requires tailored data types and adjustable parameters, enhancing the radars' adaptability and flexibility in exploration [60]. When attempting to detect faint echoes from beneath the surface of Mars, radar systems that operate at lower frequency bands with wider bandwidths can experience waveform distortions. These distortions are caused by the transmission module, antenna, and reception module, and can lead to significant differences between received signals and ideal waveforms [40,61].

To address this, measurements and simulations of the radar's transmission and reception modules, as well as antenna patterns, are required. These are then compared to the ideal signal spectrum, to compensate for waveform distortions [61,62]. During daytime surface exploration on Mars, the ionosphere can cause signal defocusing [55,63]. To mitigate this effect, the radar systems measure the total electron content of the ionosphere, to obtain compensation coefficients. Doppler analysis is also employed to achieve imaging results [64]. Additionally, the motion of the spacecraft itself can introduce signal variations. Doppler-beam sharpening techniques are utilized to compensate for motion in directions that are different from the vertical direction of the spacecraft [65,66]. Once the radar data are obtained, corresponding analysis is performed, based on the research objectives. This analysis aims to reverse the relevant electromagnetic parameters, such as dielectric permittivity and loss tangent. In Section 3, the method of reversing a subsurface material's dielectric properties using orbiter-mounted radar data will be discussed in detail.

3. The Permittivity Inversion

3.1. The Permittivity

While using spacecraft radar to detect the subsurface of Mars, the permittivity is a physical parameter we commonly apply, to determine the composition of a substance. Permittivity, as a complex number, comprises both a real part and an imaginary part [67]. The real part, known as the relative permittivity, typically influences the propagation speed of electromagnetic waves in a medium, whereas the imaginary part primarily results in energy loss during the propagation of electromagnetic waves in the medium. In this paper, when discussing the permittivity, we generally refer to its real part. Through the inversion of radar data on the permittivity of subsurface materials beneath the Martian surface, we can ascertain the nature of the subsurface materials. This method allows us to infer the properties of these subsurface materials, consequently elucidating the nature of the substances detected by radar. Through this approach, we gain a deeper understanding of the structure and composition beneath the surface of Mars, providing a foundation for further research. As we cannot directly obtain samples of subsurface materials on Mars currently, inversely deducing the permittivity can help us reasonably infer the property of subsurface materials on Mars.

3.2. The Intensity Values Collected by the Radar

Due to incomplete radar data collection at other frequencies, using MARSIS to probe the SPLDs is hindered, especially by the severely affected radar data at 3 MHz due to the ionosphere. Lauro et al. [68] adopted the more complete radar data at 4 MHz. To mitigate power variance resulting from variable roughness, Lauro et al. [68] employed the method developed by Oswald and Gogineni [69]. They derived an equation to determine the along-track waveform-averaging window from the diameter of the pulse-limited footprint, which can be expressed as [68]

$$W = 2\sqrt{c\frac{P}{2}\left(H + \frac{z}{n}\right)} \cong 2\sqrt{c\frac{P}{2}H}, \quad (1)$$

where c is the speed of light in a vacuum, p is the transmitted pulse length (in this case, $p = 1 \mu\text{s}$), and H represents the spacecraft altitude. As MARSIS radar operates on Mars, the value of H varies between 250 km and 900 km; z indicates the depth of the reflector, and n is the refractive index of water ice [68]. Utilizing the along-track waveform-averaging window, the aggregated power and the average echo power are presented in the following equation. Lauro et al. [68] calculated the intensity variability $\sigma_1(x_i)$, as indicated by

$$\sigma_1(x_i) = \frac{10}{\ln(10)} \frac{\sqrt{\frac{1}{N} \sum_{x=x_i-W/2}^{x_i+W/2} [P_{\text{ag}}(x) - \langle P_{\text{ag}}(x_i) \rangle]^2}}{\langle P_{\text{ag}}(x_i) \rangle}, \tag{2}$$

where x_i is along each orbit at the position, which here could be the surface topography or the SPLDs thickness. $P_{\text{ag}}(x)$ is the aggregated power, and the average echo power ($\langle P_{\text{ag}}(x_i) \rangle$) can be exhibited as

$$\langle P_{\text{ag}}(x_i) \rangle = \frac{1}{N} \sum_{x=x_i-W/2}^{x_i+W/2} P_{\text{ag}}(x). \tag{3}$$

Based on the intensity variability, Lauro et al. [27] obtained the intensity values gathered along the radar track. These values were then utilized to calculate the basal permittivity, using the probabilistic–inversion approach introduced by Lauro et al. [68].

3.3. Permittivity Estimated by Probabilistic-Inversion Approach

3.3.1. Ice Layer Dielectric Properties

The probabilistic-inversion approach to determining the dielectric permittivity beneath the SPLDs on Mars was employed by Lauro et al. [68]. It is necessary to understand the characteristics of the SPLDs ice layers before proceeding. Previous studies have indicated that the SPLDs are composed of a mixture of water ice and silicate powder [70], and it is generally assumed that water ice and silicate powder are distributed uniformly on the SPLDs. To explore the various compositional scenarios of the SPLDs, prior knowledge of the dielectric properties of both pure and dirty ice is required. Although the node characteristics of pure water ice can be obtained through laboratory measurements, the dielectric properties measurements of pure water ice are inconsistent, due to factors such as the cooling process, aging, bubbles, and cracks within the ice [71,72]. Therefore, Lauro et al. [68] used data from Kawada [73] to reverse the dielectric properties of the bottom of the SPLDs. For dirty ice, being a two-phase mixture, it is assumed that the content of silicate dust is 5%, 10%, 15%, or 20%. The Maxwell–Garnett mixing rule is used to determine the effective dielectric properties of the mixture [74]. Figure 3 illustrates the variation curve of the attenuation α of the 4 MHz radar wave under different volume fractions (water ice–silicate) and at different temperatures. The real-part values of the dielectric constant for ice with different volume fractions are approximately 3. This is the dielectric permittivity of typical water ice on Mars.

3.3.2. Deriving the Permittivity of the SPLDs

According to the principle that radar electromagnetic waves propagate in a subsurface layered medium, we find the ratio of the base energy to the surface energy (P_b/P_s) in the radar echo signal. The following equation can be obtained for the inversion of the dielectric permittivity, which is shown as follows [68]:

$$\frac{P_b}{P_s} = \left[\frac{(1 - \rho_s^2)\rho_b}{\rho_s} \right]^2 e^{-4\alpha_{ie}\tau_{ie}v_{ie}}, \tag{4}$$

where ρ_s, ρ_b are the Fresnel reflection coefficients at the interfaces air/surface and ice-layer/basal material, and

$$\rho_s = \frac{1 - \sqrt{\epsilon_{ie}}}{1 + \sqrt{\epsilon_{ie}}}, \tag{5}$$

$$\rho_b = \frac{\sqrt{\epsilon_{ie}} - \sqrt{\epsilon_b}}{\sqrt{\epsilon_{ie}} + \sqrt{\epsilon_b}} \tag{6}$$

where ϵ_b is the permittivity of the basal material underlying the SPLDs. Lauro et al. [68] employed the probability density function (PDF) of the measured data and the model parameters as inputs to solve the inversion of the equation. However, this approach requires making the following assumptions about the ice layer [68]:

1. The ice layer consists of a uniform mixture of water ice and silicate, with the volume fraction of silicate (f_v) within the range of [0.05, 0.2].
2. The temperature $T(z)$ of the ice layer linearly increases with depth, with the surface temperature T_s at 160 K and the basal temperature T_b within the range of 170 K to 270 K.
3. Different values of f_v and $T(z)$ will influence the value of ϵ_{ice} .

A detailed derivation of the procedure for calculating the permittivity of the basal material underlying the SPLDs can be found in Lauro et al. [68].

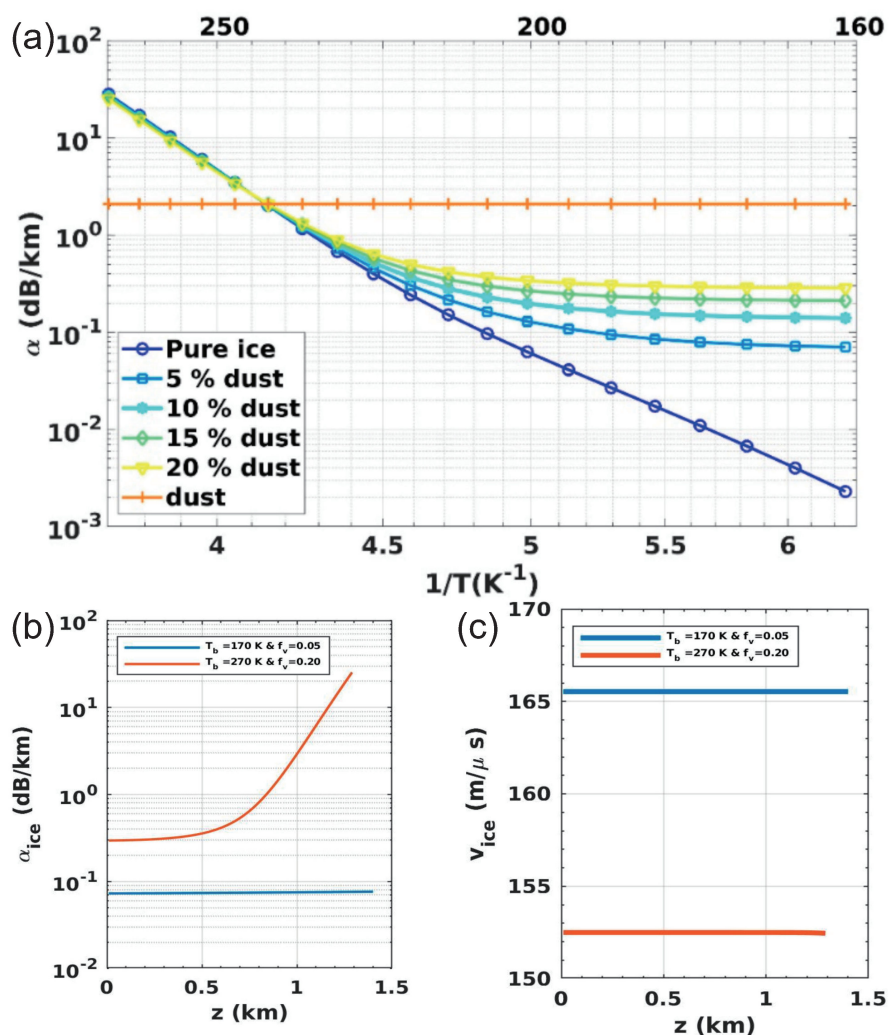


Figure 3. (a) The variation in the attenuation coefficient with temperature at 4 MHz across various materials, such as SPLDs. (b) Laboratory measurements of the attenuation characteristics of water ice. (c) Velocity profiles within the ice layer for the extreme parameter values investigated in the model’s range, adopted from Lauro et al. [68].

4. Current Existence of Liquid Water on Mars

4.1. Discovery of Liquid Water on Mars

Since the activation of MARSIS and SHARAD, numerous pieces of evidence related to the presence of water ice on Mars have been detected over the past few decades [51,75,76]. Water ice on Mars is predominantly found in layered deposits beneath the polar ice caps [19]. In recent years, the MARSIS radar identified a region of bright radar reflections at the base of Ultimi Scopuli (193° E, 81° S) in the Martian South Pole region [26]. In Figure 4a, two distinct interfaces are visible: the continuous upper interface corresponds to the surface echo, while the lower interface at approximately 160 μs corresponds to the basal echo of the SPLDs. Additionally, within this interface, partial bright radar reflections can be observed [26]. By constructing a model that assumes the proportion of water ice and dust in the SPLDs, as well as the vertical temperature variation within the SPLDs, the calculated results show a region with a basal temperature of approximately 205 K and a permittivity greater than 15 (Figure 4e). This leads to the inference that the region probably corresponds to highly chlorinated brine [26]. The presence of highly chlorinated brine, which significantly depresses the freezing point of water, suggests the potential existence of liquid water on Mars. Applying signal-processing techniques commonly used for Earth’s polar ice sheets, Lauro et al. [27] employed the mesh–refinement technique to obtain a permittivity map beneath the SPLDs. Lauro et al. [27] identified multiple bright regions, and regions with permittivity greater than 15 were interpreted as potential areas of liquid water presence. This led to the hypothesis that multiple liquid-water bodies could exist beneath the SPLDs [27].

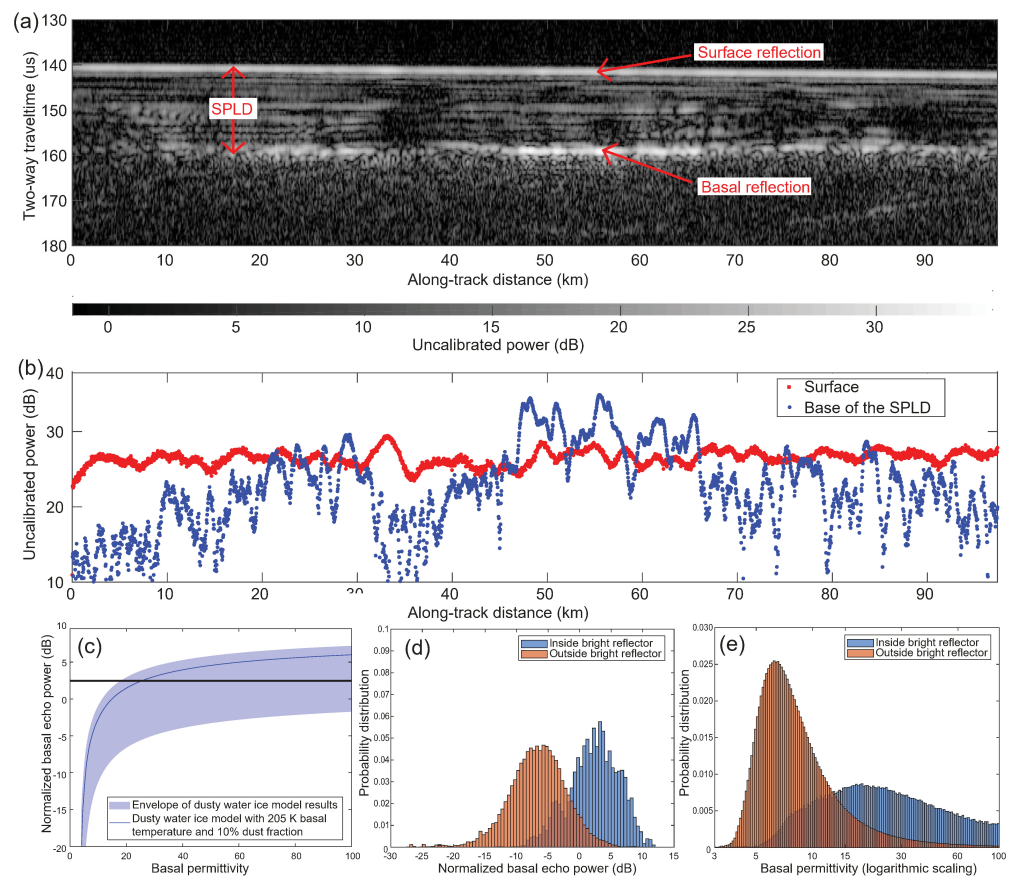


Figure 4. Radar–observed evidence of liquid water under Mars’ south polar ice cap, adopted from Orosei et al. [26]: (a) Radar imagery depicting MARSIS orbit 10737. (b) A graphical representation of surface and basal echo power. (c) Electromagnetic simulation results calculated at 4 MHz. (d) Comparative distributions of normalized basal echo power within and beyond the high–reflection area. (e) Permittivity distributions at the basal layer inside and outside the high–reflection area.

4.2. Dispute on the Existence of Liquid Water on the SPLDs

Radar observations have indicated the presence of multiple buried bodies of liquid water under the Martian south polar ice cap [26,27]. However, there are also numerous opposing viewpoints regarding the presence of liquid water in this region. Some argue that the bright radar reflections could be caused by factors other than a liquid-water body. Debates among researchers have ensued, regarding the composition of the underlying material in this area. The question of whether liquid water exists in this region undoubtedly remains a focal point in current Mars research. We summarize the latest findings on the debate on liquid water under the Martian south polar ice cap. Figure 5 illustrates the relevant debate.

4.2.1. Local Environmental Factors May Not Support the Existence of Liquid Water

Some viewpoints suggest that under the typical current conditions on Mars, the pressure and temperature at the SPLDs base do not support the formation of liquid water [28]. Sori and Bramson [77] constructed a heat-flux model for the SPLDs, based on the estimated basal permittivity by Orosei et al. [26], shown in Figure 6. They calculated that for the existence of liquid water, at least 72 mW/m^2 of heat flux would be required [77]. However, the current global average heat flux on Mars is around 19 mW/m^2 , with a range of $14\text{--}25 \text{ mW/m}^2$ [78–80]. Additionally, there has been no recent geological activity near the South Pole to provide the necessary heat, making it challenging for liquid water to exist at the base [77].

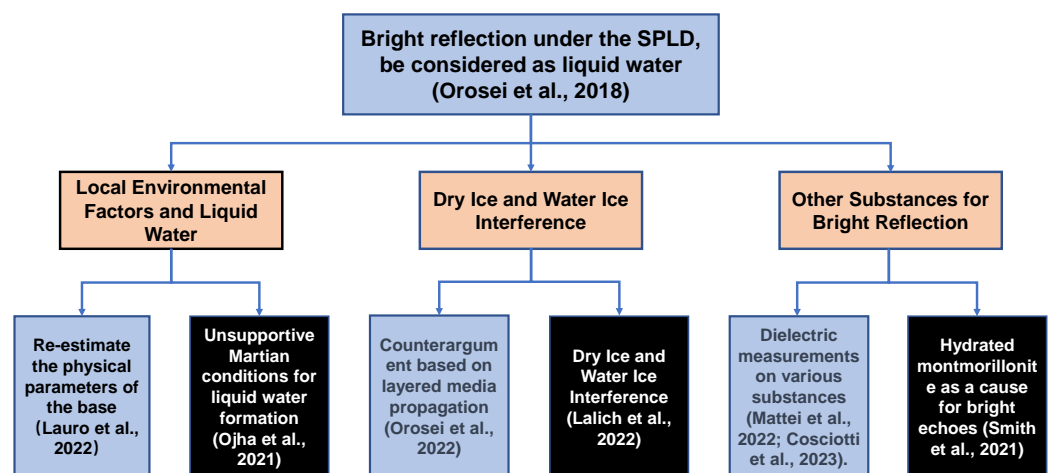


Figure 5. The latest research debate on the existence of liquid water on the SPLDs. The black boxes are negative views on the presence of water at the South Pole of Mars, and the blue boxes are the response to the negative views [26,28,30–33,81,82].

To address this issue, Lauro et al. [81] optimized the estimates for the basal temperature and permittivity by analyzing signal attenuation using MARSIS frequencies of 3 MHz, 4 MHz, and 5 MHz, respectively. They estimated the surface temperature and heat flux of the SPLDs and they utilized the Maxwell–Garnett mixing formula. As a result, they re-calculated the basal permittivity to be approximately 40, with a loss-tangent value of 0.0017 and a maximum temperature potential of 240 K, as shown in Figure 7. Based on the deduced permittivity values and temperature, they suggested that the material in this area of liquid water is reasonable and could be rich in brine [81].

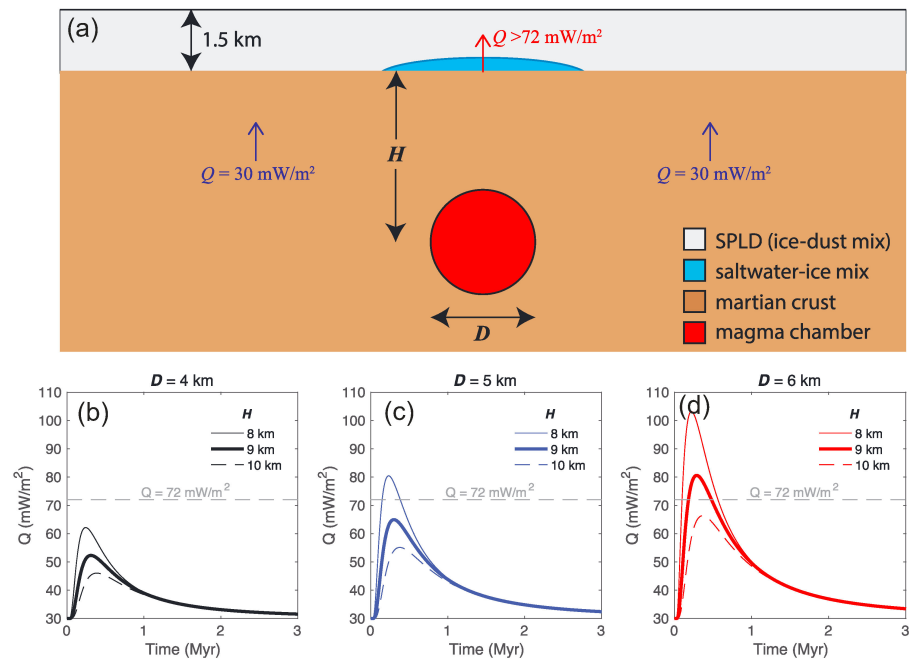


Figure 6. Schematic diagram of a model of heat flow under the Martian south polar ice cap, adopted from Sori and Bramson [77]: (a) Diagram illustrating a scenario resulting in a localized increase in heat flux beneath the SPLDs. D represents the diameter of the magma chamber, H signifies the depth to the center of the chamber, and Q is set at 30 mW/m^2 , representing the ambient geothermal heat flux. (b–d) Presentation of the relationships between Q and various combinations of D and H .

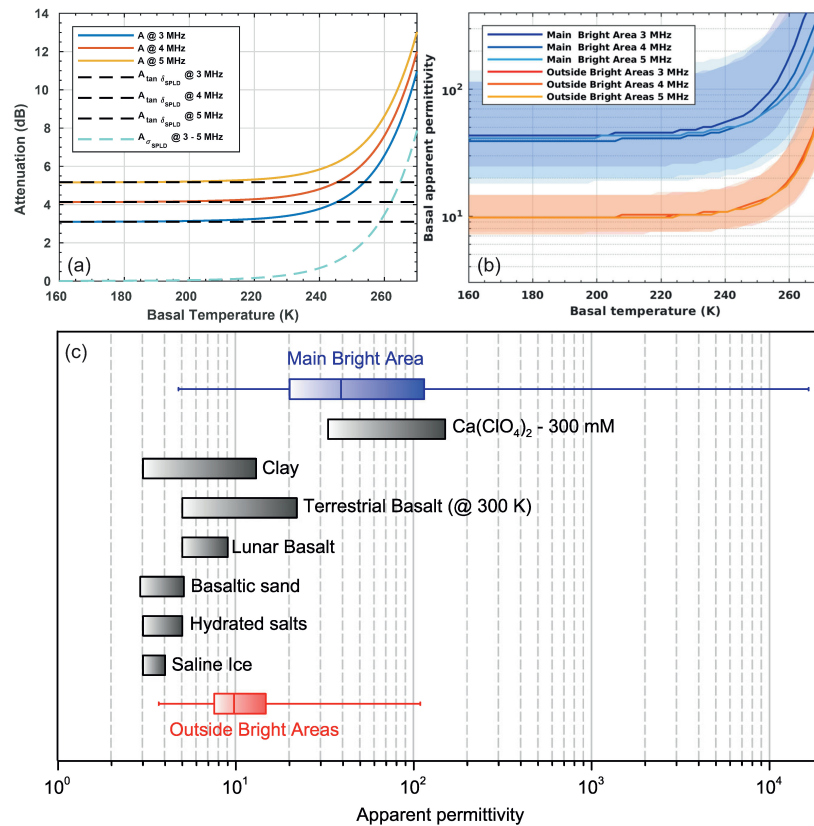


Figure 7. (a) Analysis of attenuation within an ice and dust composite at MARSIS frequencies. (b) Variation in apparent basal permittivity, both inside and outside the high-reflective region. (c) Apparent permittivity of different materials [81].

4.2.2. CO₂-Ice and Water-Ice Interference with Echoes

Lalich et al. [31] conducted simulations of three different subsurface structures of SPLDs (Figure 8a). The first scenario involved a water-ice layer without a layer of CO₂ ice, serving as a reference. The second scenario included a layer of CO₂ ice with a thickness ranging from 1 to 100 m between water ice and bedrock. The third scenario featured two layers of CO₂ ice between water-ice layers. They simulated the waveforms generated by each scenario and compared these simulations with observations detected by MARSIS. They found that the simulation produced in the third scenario exhibited strong similarity to the observation detected by MARSIS (Figure 8b). Therefore, they concluded that the bright radar echoes detected by MARSIS are likely a result of interference between the CO₂ ice and water ice, shown in Figure 8 [31]. However, Orosei et al. [82] evaluated the echoes generated by the simulated subsurface structures, using the theoretical framework of layered media propagation. Orosei et al. [82] argued that in such terrain structures involving coherent interference between layers, the interference produced by radar waves at one frequency cannot have the same effect at another frequency. Therefore, they countered the possibility that the bright echoes were caused by the interference of CO₂-ice and water-ice layers [82].

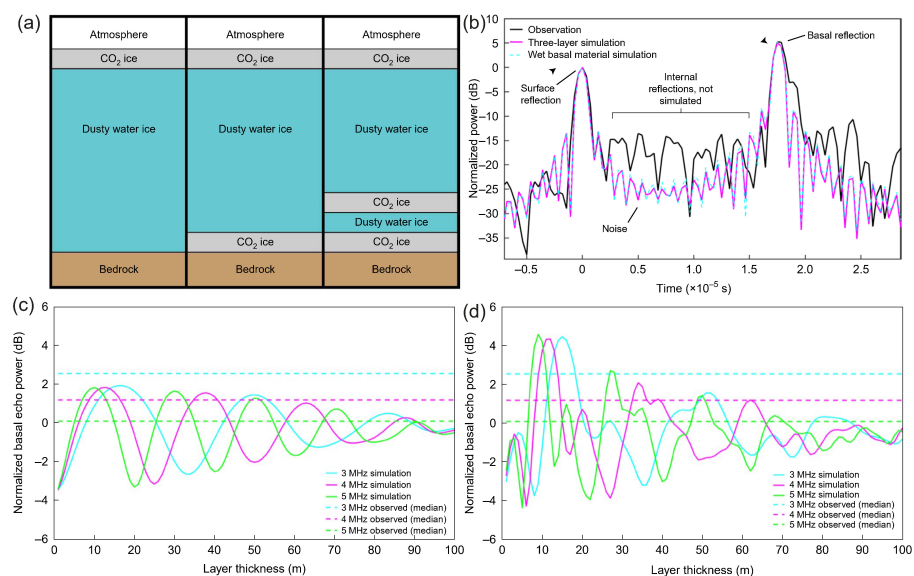


Figure 8. Modeling and simulations of subglacial structures at the South Pole of Mars, adopted from Lalich et al. [31]: (a) Schematic illustrations depicting three simulated scenarios. (b) A comparison between MARSIS echoes observed in reality and those simulated at 4 MHz. (c) Simulation with a single CO₂ ice layer. (d) Simulation with two CO₂ ice layers.

In addition, Lauro et al. [83] focused on three key aspects—namely, the electromagnetic model, dielectric properties, and materials and geology—to address the simulation:

1. **Electromagnetic Model:** In response to the findings by Lalich et al. [31], suggesting the third scenario as a potential cause for bright echoes, Lauro et al. [83] conducted experiments employing this scenario as a model, with the exclusion of the non-existent CO₂-ice layer above. Deviating from the original model, they observed that the Normalized Basal Echo Power (NBEP) values at the radar’s three frequencies (3, 4, 5 MHz) did not simultaneously reach their maximum at the same thickness of the dry-ice layer. Instead, comparable NBEP values (approximately 4.55 dB) were attained only when the radar frequencies corresponded to thicknesses of 15.4 m, 11.4 m, and 9 m, respectively.
2. **Dielectric Properties:** Lalich et al. [31] utilized dry-ice permittivity values from Pettinelli et al. [84] in their simulation. However, Lauro et al. [83] contested the accuracy of the data interpretation from that particular article, asserting a misinterpretation leading to the citation of incorrect permittivity values.

- Materials and Geology: Contrary to Lalich et al. [31]’s simulation, which suggested that Ultimi Scopuli’s surface is covered by the residual-ice-cap unit (RIC) rather than the seasonal-ice-cap unit (SIC), Lauro et al. [83] argued that, in reality, the significant distance of approximately 400 km between the center of the Antarctic RIC and Ultimi Scopuli makes it implausible for the RIC to cover the surface of Ultimi Scopuli. Accordingly, they proposed that the surface of Ultimi Scopuli should be influenced by the SIC, with its CO₂-ice layer exhibiting periodic changes corresponding to the seasons.

4.2.3. Other Possibilities Causing the Bright Reflection

Smith et al. [30] propose that hydrated montmorillonite could also lead to bright echo reflections. They selected the common Ca-montmorillonite found on Mars as a sample, fully hydrating it to create a plastic paste-like substance. They performed dielectric measurements on the hydrated sample and discovered that at 230 K and a central frequency range of 3–5 MHz, the dielectric constant ranged from 15 to 25, accompanied by a loss tangent of 1.2 to 1.4, shown in Figure 9a,b. As montmorillonite is prevalent on Mars, they suggested that the bright echo reflection could be more reasonably attributed to hydrated montmorillonite than to a liquid-water body [30]. Additionally, some viewpoints propose that the radar-detected regions of liquid water might be conductive or semiconductive minerals, such as hematite or hydrated minerals like jarosite, which could also explain the bright reflection at the base [29].

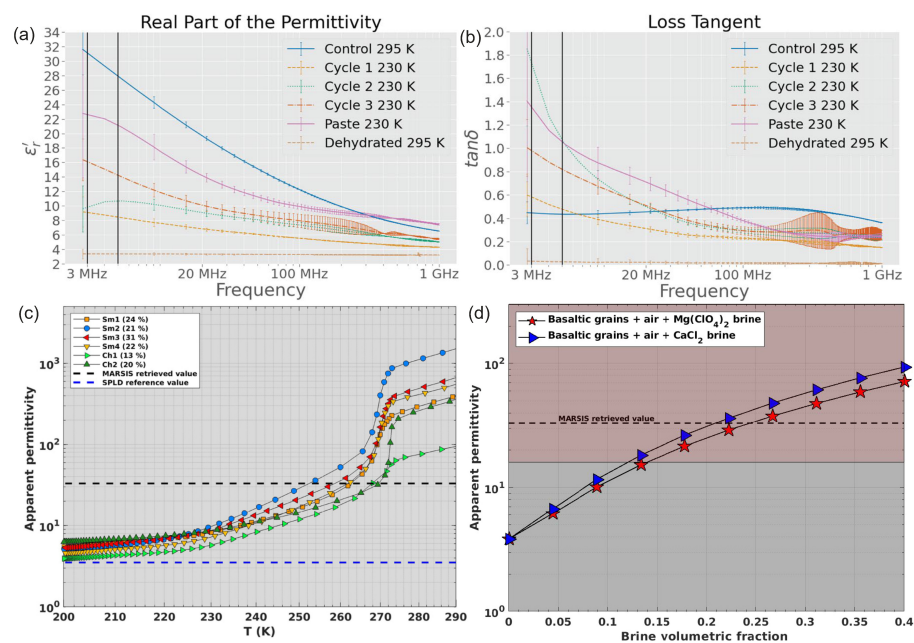


Figure 9. The relationship between apparent permittivity (a) and the loss tangent (b) with various samples and frequencies [30]. (c) The dependence of apparent permittivity on different temperatures and various sample types. (d) The influence of brine content on the apparent permittivity of soil, as determined through CRIM simulations at 4 MHz, as presented in Mattei et al. [32].

Mattei et al. [32] conducted dielectric measurements on different levels of water content, clay content, and various types of minerals. They found that the apparent permittivity of clay deposits did not exceed 7 at 203 K and that significant effects on clay’s dielectric properties only occurred at temperatures above 250 K (Figure 9c). Additionally, they measured the apparent permittivity of Mg(ClO₄)₂ and CaCl₂ brines with different volume fractions and found that certain volume fractions of these brines could achieve the apparent permittivity values required for MARSIS inversion (Figure 9d). Therefore, they argued that, compared to other substances like minerals or clay, high-concentration brines are better suited to explaining the bright reflection at the the SPLDs base [32]. On the other

hand, Cosciotti et al. [33] replicated experiments measuring the dielectric properties of clay samples. They found that even in clay samples with high moisture content, the apparent permittivity exhibited was only 8.4 at 4 MHz and 230 K, and it was only 4.1 at 200 K. These values were significantly lower than the actual inverted values. This research has conclusively demonstrated that materials such as clays cannot produce the strong reflections observed by MARSIS [33].

In the various studies mentioned above, the researchers supporting the presence of liquid water at the base of the SPLDs have responded to every argument against the existence of liquid water. Currently, researchers who do not support the presence of liquid water at the base of the SPLDs have not yet responded to these latest arguments. Therefore, we maintain an optimistic outlook regarding the existence of liquid water at the base of the SPLDs. The future radar payloads on Mars could provide additional observations of the region, to validate the presence of liquid water and enhance the robustness of these findings.

5. The Discovery of Liquid Water Provides Insights for the Exploration of Martian Life

5.1. Life in Extreme-Cryogenic-Brine Ecosystems

The discovery of liquid water beneath the Martian south polar ice cap provides crucial clues regarding the current potential for life on Mars and points the way for future astrobiological research [85]. Orosei et al. [26] suggests the presence of highly concentrated perchlorate brine beneath the SPLDs base. The SPLDs basal temperature could reach a maximum of 240 K [81]. Therefore, the question arises: what kind of life could exist in the extreme environment beneath the ice layer, characterized by anaerobic, sunlight-deprived, cold conditions with high concentrations of perchlorates?

Micro-organisms on Earth can survive in low-temperature, oxygen-deprived environments, as has already been discovered. The micro-organisms in the saltwater Lake Vida, located in the Antarctic region, are completely enclosed by a permanent ice cover, as shown in Figure 10 [86,87]. The lake's temperature is minus 13 degrees Celsius and, due to its ice-covered state, it also lacks sunlight and oxygen [88]. In addition to low temperatures, the high concentration of perchlorates in the environment restricts most potential microbial species. Most micro-organisms cannot adapt to such high perchlorate concentrations. Although the high perchlorate concentrations in Earth's natural environment cannot reach the levels found in the SPLDs liquid-water bodies on Mars [89], environments on Earth with high concentrations of salt can still provide insights into the tolerance of micro-organisms to salt. Prior to the discovery of possible liquid water beneath the SPLDs ice layer, halophiles were considered the most likely candidates for microbial life on Mars, due to their ability to survive in extreme high-salinity environments [26,90,91]. Some halophiles can even survive in concentrated brines for short periods [92–94], and certain halophiles can exist in sub-zero cold environments [90,95], such as halobacterium lacusprofundi (*H. lacusprofundi*), isolated from a deep lake in Antarctica [96]. The Atacama Desert, one of the harshest environment on Earth, which includes different salt flats, is a suitable environment to research. Aerts et al. [97] used sophisticated extraction procedures to detect and analyze the amino acids from the salt flats. They found that the majority of samples contained diverse and complex microbial communities, with a large portion being halophilic bacteria. In addition, they found that the growth of the micro-organism was not hindered by salt, as they could adapt to higher concentrations of saline environment. Therefore, halophiles are one of the most likely candidates for microbial life beneath the SPLDs ice layer. As samples from beneath the SPLDs ice layer cannot currently be obtained, we need to determine whether micro-organisms can survive, thereby simulating the corresponding environment in Earth's laboratory. DasSarma et al. [91] cultured *H. lacusprofundi* and *Halobacterium* sp. NRC-1 in a 40 mM (here nM is the molarity, 1 nM = 1 nmol/L) perchlorate environment under dark and oxygen-deprived conditions. They recorded the bacterial counts of both strains at zero and eight days and found that *H. lacusprofundi* was capable of growth in a high-perchlorate environment compared to other haloarchaea.

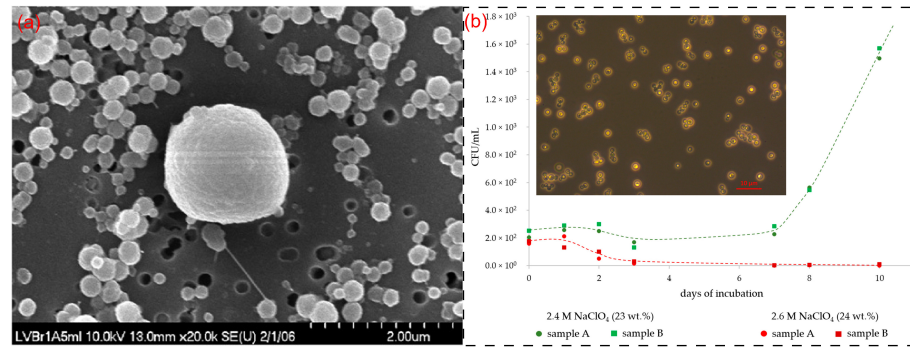


Figure 10. (a) Image of micro-organisms found in Lake Vida [87]. (b) Growth curves of *D. hansenii* in liquid growth media at a temperature of 25 degrees Celsius [89].

Additionally, DasSarma et al. [91] placed *H. lacusprofundi* and *Halobacterium* sp. NRC-1 in culture media containing different ions and observed the growth rates of the two strains. They discovered that [91]:

1. *H. lacusprofundi* can adapt to higher concentrations of perchlorates, with less inhibition of growth, by increasing perchlorate concentrations within the 0–2 M range, compared to other haloarchaea.
2. Divalent cations have a greater impact on microbial growth rates than monovalent cations.
3. Perchlorate ions have a more significant impact on microbial growth rates than cations.

DasSarma et al. [91] concluded that although perchlorates can inhibit the growth of *H. lacusprofundi*, the currently assumed high-perchlorate concentrations on Mars would not be sufficient to completely inhibit its growth. Heinz et al. [89] discovered *Debaryomyces hansenii* and *Purpureocillium lilacinum*, the highest perchlorate-tolerant micro-organisms reported in all studies to date. To study eukaryotic organisms' tolerance to perchlorates, they cultured *Debaryomyces hansenii* and *Purpureocillium lilacinum* separately in liquid growth media with varying concentrations of sodium perchlorate. They found that *Debaryomyces hansenii* can grow in a 2.4 mol/L NaClO₄ environment, while all cells die after 10 days in a 2.6 mol/L NaClO₄ environment (Figure 10b).

5.2. Exploring the Potential Existence of Life on Mars

The suitable way to determine if micro-organisms exist in the SPLDs region is to analyze samples collected from this area. However, the SPLDs region is located approximately 1.5 km below the Martian surface [26]. Therefore, it is currently extremely challenging to directly obtain samples from this area. As of now, obtaining surface samples from Mars is most likely through robotic missions or automated spacecraft equipped with sample collection tools. CNSA, NASA, and ESA all have corresponding Mars sampling programs. For example, ESA has proposed a staged plan to collect samples from Mars and return them to Earth, shown in Figure 11. China's Tianwen-3 mission plans to collect surface samples from Mars and gather data from the surrounding environment [98]. The Tianwen-3 mission includes two major components [99]: one for landing and collecting Mars samples (lander) and one that will work on the satellite orbit (orbiter). The landing spacecraft will collect samples itself and send the collected samples back to the orbiter with its ascent vehicle. After docking with the ascent vehicle, the orbiter will carry the samples back to Earth. Two Long March 5 rockets will be used to launch the Tianwen-3 spacecraft. The orbiter will launch in 2028, arrive in August or September 2029, and return in October 2030 [99]. There are two planned missions regarding the timing of the lander launching and touching down. In plan A, the lander will launch in December 2028 and arrive on Mars in July 2029, and it will take about 6 months to collect samples. To avoid winter in the northern hemisphere, plan B proposes launching in May 2028 and landing in August 2030, then spending about three months collecting samples [99]. While collecting samples, a mini-helicopter and a four-legged robot could be used to detect the surrounding environment and collect the

intimately connected to it. Water provides the fundamental conditions for the survival of organisms, acting as both a reactant in various biological processes and a solvent for these reactions within organisms. Over the past few decades of research, evidence has suggested the past existence of liquid water on Mars and, in recent years, water ice has been discovered in regions such as the Martian poles. Since the discovery of liquid water beneath the south polar ice cap of Mars by Orosei et al. [26] in 2018 the presence of liquid water on Mars has become one of the hottest topics in Martian exploration. The discovery of liquid water at the base of the SPLDs on Mars and the summary of implications for Mars life studies are as follows:

1. MARSIS detected bright radar echoes at the base of the SPLDs, and analysis indicates that these echoes were caused by a water body containing a high concentration of perchlorates. While there have been doubts suggesting that the bright radar echoes could be due to substances such as clay, simulations of the dielectric properties of relevant materials suggest that clay cannot produce such bright reflections. These studies suggest the likely presence of liquid water at the base of the SPLDs on Mars, albeit containing a significant amount of perchlorates.
2. The presence of liquid water implies the possibility of microbial life. The high salinity, low temperature, and anaerobic conditions at the base of the Mars SPLDs seem unfavorable for the long-term survival of life. Research on similar extreme environments on Earth and laboratory experiments demonstrating the survival of halophilic bacteria in simulated extreme conditions suggest that if microbial life exists at the base of the Mars SPLDs, it is most likely to be halophilic bacteria.
3. Additionally, studies of carbon-containing meteorites on Earth have shown that these meteorites may produce organic compounds under the influence of water and heat, which could potentially support microbial life. Mars has also been extensively impacted by meteorites, and similar reactions might have occurred on Mars. This provides insights for the selection of sampling sites and specimens in Mars sampling missions.

In future studies, the deployment of advanced radar systems to enable more precise observations of this region, along with the collection of additional data to improve the accuracy of dielectric properties inversion beneath the ice layers, could be considered valuable avenues for exploration. In addition, exploration of the Martian-North-Pole region, which also features substantial ice deposits, could provide insight into whether similar bright reflections exist there. Furthermore, laboratory investigations of future Martian soil samples could enhance our understanding of Martian soil composition, aiding in better predicting the constituents of the SPLDs base. The presence of liquid water on the subsurface of Mars implies the potential for the existence of micro-organisms. By combining this discovery with the surrounding Martian environment, we can more reasonably speculate about the possibility of and potential forms of life on Mars. The identification of liquid water will impact our Mars-exploration strategies, resulting in a heightened emphasis on observing liquid water and a more precise collection of soil samples. Moreover, studying how extremophiles survive in Earth's extreme environments might offer valuable insights for studying potential Martian life, providing us with additional strategies for searching for life on Mars.

This paper provides a comprehensive summary of recent research on the liquid water at the base of the SPLDs on Mars and studies related to Martian micro-organisms. Including orbital radar exploration of the Martian subsurface and investigations into the survival of micro-organisms in simulated Martian environments, the paper covers various aspects of recent advancements in the study of Martian water bodies and micro-organisms. We believe that this paper will serve as a valuable reference for future orbital-radar exploration of Martian-subsurface water bodies, while also offering insights for the selection of sampling sites in China's Tianwen-3 mission.

Author Contributions: Conceptualization, C.D.; methodology, J.Z. and C.D.; software, J.Z. and C.D.; validation, J.Z., C.D., S.X., and Y.S.; formal analysis, J.Z., C.D., S.X., S.Y., J.L., M.C., and S.D.; investigation, J.Z., C.D., S.X., S.Y., J.L., M.C., and S.D.; resources, C.D. and S.Y.; data curation, C.D.; writing—original draft preparation, J.Z. and C.D.; writing—review and editing, C.D., S.X., S.Y., J.L., M.C., and S.D.; visualization, C.D.; project administration, C.D.; supervision, C.D. funding acquisition, C.D. and S.Y. All authors have read and agreed to the published version of the manuscript.

Funding: This work was supported by the National Natural Science Foundation of China (Grant No. 42241139, 62227901 and 42004099), the Opening Fund of the Key Laboratory of Lunar and Deep Space Exploration, Chinese Academy of Sciences (No. LDSE202005), the National Innovation and Entrepreneurship Training Program for College Students (No. 202310590016), the Fund of Shanghai Institute of Aerospace System Engineering (No. PZ_YY_SYF_JY200275), and the Shenzhen Municipal Government Investment Project (No. 2106_440300_04_03_901272).

Data Availability Statement: No new data was generated for this paper.

Acknowledgments: We would like to thank Roberto Orosei for his suggestions and discussion on this work. This was supported by the team “Searching For Subglacial Water On Mars With Orbiting Ground Penetrating Radars” of the International Space Science Institute (ISSI).

Conflicts of Interest: The authors declare no conflicts of interest.

References

1. Mckay, C.P. The search for life on Mars. *Orig. Life Evol. Biosph.* **1997**, *27*, 263–289. [[CrossRef](#)]
2. Schulze-Makuch, D.; Fairén, A.G.; Davila, A.F. The case for life on Mars. *Int. J. Astrobiol.* **2008**, *7*, 117–141. [[CrossRef](#)]
3. Elson, B. Venus Project Team Finds Extensive Volcanic Activity. *Aviat. Week Space Technol.* **1984**, *102*, 44–45.
4. Schaber, G.G.; Kozak, R.C.; Masursky, H. Cleopatra Patera on Venus: Venera 15/16 evidence for a volcanic origin. *Geophys. Res. Lett.* **1987**, *14*, 41–44. [[CrossRef](#)]
5. Davidson, G.T.; Anderson, A.D. Venus: Volcanic eruptions may cause atmospheric obscuration. *Science* **1967**, *156*, 1729–1730. [[CrossRef](#)] [[PubMed](#)]
6. Chicarro, A. Mars Express mission and astrobiology. *Sol. Syst. Res.* **2002**, *36*, 487–491. [[CrossRef](#)]
7. Grady, M.M. WatSen: Searching for clues for water (and life) on Mars. *Int. J. Astrobiol.* **2006**, *5*, 211–219. [[CrossRef](#)]
8. Checinska Sielaff, A.; Smith, S.A. Habitability of mars: How welcoming are the surface and subsurface to life on the red planet? *Geosciences* **2019**, *9*, 361. [[CrossRef](#)]
9. Brack, A.; Pillinger, C.T.; Sims, M.R. The Beagle 2 Lander and the Search for Traces of Life on Mars. In *Life in the Universe: From the Miller Experiment to the Search for Life on Other Worlds*; Springer: Dordrecht, The Netherlands, 2004; pp. 227–231.
10. Langhoff, S.R. *Workshop Report on Deep Mars: Accessing the Subsurface of Mars on Near Term Missions*; NASA/CP-2008-214586; NASA: Washington, DC, USA, 2008.
11. Voosen, P. Mars rover steps up hunt for molecular signs of life. *Science* **2017**, *355*, 444–445. [[CrossRef](#)]
12. Carr, M.H. Water on mars. *Nature* **1987**, *326*, 30–35. [[CrossRef](#)]
13. McEwen, A.S.; Hansen, C.; Delamere, W.A.; Eliason, E.; Herkenhoff, K.E.; Keszthelyi, L.; Gulick, V.; Kirk, R.L.; Mellon, M.; Grant, J.A.; et al. A closer look at water-related geologic activity on Mars. *Science* **2007**, *317*, 1706–1709. [[CrossRef](#)] [[PubMed](#)]
14. Mustard, J.F.; Murchie, S.L.; Pelkey, S.; Ehlmann, B.; Milliken, R.; Grant, J.A.; Bibring, J.P.; Poulet, F.; Bishop, J.; Dobrea, E.N.; et al. Hydrated silicate minerals on Mars observed by the Mars Reconnaissance Orbiter CRISM instrument. *Nature* **2008**, *454*, 305–309. [[CrossRef](#)]
15. Graf, J.E.; Zurek, R.W.; Eisen, H.J.; Jai, B.; Johnston, M.; DePaula, R. The Mars reconnaissance orbiter mission. *Acta Astronaut.* **2005**, *57*, 566–578. [[CrossRef](#)]
16. Orosei, R.; Ding, C.; Fa, W.; Giannopoulos, A.; Hérique, A.; Kofman, W.; Lauro, S.E.; Li, C.; Pettinelli, E.; Su, Y.; et al. The global search for liquid water on Mars from orbit: Current and future perspectives. *Life* **2020**, *10*, 120. [[CrossRef](#)] [[PubMed](#)]
17. Orosei, R.; Jordan, R.; Morgan, D.; Cartacci, M.; Cicchetti, A.; Duru, F.; Gurnett, D.; Heggy, E.; Kirchner, D.; Noschese, R.; et al. Mars Advanced Radar for Subsurface and Ionospheric Sounding (MARSIS) after nine years of operation: A summary. *Planet. Space Sci.* **2015**, *112*, 98–114. [[CrossRef](#)]
18. Putzig, N.E.; Seu, R.; Morgan, G.A.; Smith, I.B.; Campbell, B.A.; Perry, M.R.; Mastrogioseppe, M. Science results from sixteen years of MRO SHARAD operations. *Icarus* **2023**, *405*, 115715. [[CrossRef](#)]
19. Byrne, S. The polar deposits of Mars. *Annu. Rev. Earth Planet. Sci.* **2009**, *37*, 535–560. [[CrossRef](#)]
20. Langevin, Y.; Poulet, F.; Bibring, J.P.; Schmitt, B.; Douté, S.; Gondet, B. Summer evolution of the north polar cap of Mars as observed by OMEGA/Mars express. *Science* **2005**, *307*, 1581–1584. [[CrossRef](#)]
21. Picardi, G.; Seu, R.; Frigeri, A.; Melacci, P. Subsurface Sounding in “Mars Advanced Radar for Subsurface and Ionosphere Sounding” (MARSIS). *Geochim. Cosmochim. Acta Suppl.* **2005**, *69*, A531.
22. Plaut, J.J.; Picardi, G.; Safaefinili, A.; Ivanov, A.B.; Milkovich, S.M.; Cicchetti, A.; Kofman, W.; Mouginot, J.; Farrell, W.M.; Phillips, R.J.; et al. Subsurface radar sounding of the south polar layered deposits of Mars. *Science* **2007**, *316*, 92–95. [[CrossRef](#)]

23. Fan, M.; Lyu, P.; Su, Y.; Du, K.; Zhang, Q.; Zhang, Z.; Dai, S.; Hong, T. The Mars orbiter subsurface investigation radar (MOSIR) on China's Tianwen-1 mission. *Space Sci. Rev.* **2021**, *217*, 8. [[CrossRef](#)]
24. Hong, T.; Su, Y.; Fan, M.; Dai, S.; Lv, P.; Ding, C.; Zhang, Z.; Wang, R.; Liu, C.; Du, W.; et al. Flight Experiment Validation of Altitude Measurement Performance of MOSIR on Tianwen-1 Orbiter. *Remote Sens.* **2021**, *13*, 5049. [[CrossRef](#)]
25. Qiu, X.; Ding, C. Radar Observation of the Lava Tubes on the Moon and Mars. *Remote Sens.* **2023**, *15*, 2850. [[CrossRef](#)]
26. Orosei, R.; Lauro, S.E.; Pettinelli, E.; Cicchetti, A.; Coradini, M.; Cosciotti, B.; Di Paolo, F.; Flamini, E.; Mattei, E.; Pajola, M.; et al. Radar evidence of subglacial liquid water on Mars. *Science* **2018**, *361*, 490–493. [[CrossRef](#)] [[PubMed](#)]
27. Lauro, S.E.; Pettinelli, E.; Caprarelli, G.; Guallini, L.; Rossi, A.P.; Mattei, E.; Cosciotti, B.; Cicchetti, A.; Soldovieri, F.; Cartacci, M.; et al. Multiple subglacial water bodies below the south pole of Mars unveiled by new MARSIS data. *Nat. Astron.* **2021**, *5*, 63–70. [[CrossRef](#)]
28. Ojha, L.; Karimi, S.; Buffo, J.; Nerozzi, S.; Holt, J.W.; Smrekar, S.; Chevrier, V. Martian mantle heat flow estimate from the lack of lithospheric flexure in the south pole of Mars: Implications for planetary evolution and basal melting. *Geophys. Res. Lett.* **2021**, *48*, e2020GL091409. [[CrossRef](#)]
29. Bierson, C.; Tulaczyk, S.; Courville, S.; Putzig, N. Strong MARSIS radar reflections from the base of Martian south polar cap may be due to conductive ice or minerals. *Geophys. Res. Lett.* **2021**, *48*, e2021GL093880. [[CrossRef](#)]
30. Smith, I.; Lalich, D.; Rezza, C.; Horgan, B.; Whitten, J.; Nerozzi, S.; Holt, J. A solid interpretation of bright radar reflectors under the Mars south polar ice. *Geophys. Res. Lett.* **2021**, *48*, e2021GL093618. [[CrossRef](#)]
31. Lalich, D.; Hayes, A.; Poggiali, V. Explaining bright radar reflections below the south pole of Mars without liquid water. *Nat. Astron.* **2022**, *6*, 1142–1146. [[CrossRef](#)]
32. Mattei, E.; Pettinelli, E.; Lauro, S.E.; Stillman, D.E.; Cosciotti, B.; Marinangeli, L.; Tangari, A.C.; Soldovieri, F.; Orosei, R.; Caprarelli, G. Assessing the role of clay and salts on the origin of MARSIS basal bright reflections. *Earth Planet. Sci. Lett.* **2022**, *579*, 117370. [[CrossRef](#)]
33. Cosciotti, B.; Mattei, E.; Brin, A.; Lauro, S.E.; Stillman, D.E.; Cunje, A.; Hickson, D.; Caprarelli, G.; Pettinelli, E. Can clay mimic the high reflectivity of briny water below the Martian SPLD? *J. Geophys. Res. Planets* **2023**, *128*, e2022JE007513. [[CrossRef](#)]
34. Nielsen, E. Mars express and MARSIS. *Space Sci. Rev.* **2004**, *111*, 245–262. [[CrossRef](#)]
35. Picardi, G.; Biccari, D.; Seu, R.; Plaut, J.; Johnson, W.; Jordan, R.; Safaeinili, A.; Gurnett, D.; Huff, R.; Orosei, R.; et al. MARSIS: Mars advanced radar for subsurface and ionosphere sounding. In *Mars Express: The Scientific Payload*; ESA Publications Division: Noordwijk, The Netherlands, 2004; Volume 1240, pp. 51–69.
36. Biccari, D.; Picardi, G.; Seu, R.; Orosei, R.; Melacci, P.T. Mars orbital laser altimeter and Mars advanced radar for subsurface and ionosphere sounding (MARSIS). In *Electronic Imaging and Multimedia Technology III*; SPIE: Bellingham, WA, USA, 2002; Volume 4925, pp. 10–17.
37. Picardi, G.; Biccari, D.; Seu, R.; Marinangeli, L.; Johnson, W.; Jordan, R.; Plaut, J.; Safaeinili, A.; Gurnett, D.; Ori, G.G.; et al. Performance and surface scattering models for the Mars Advanced Radar for Subsurface and Ionosphere Sounding (MARSIS). *Planet. Space Sci.* **2004**, *52*, 149–156. [[CrossRef](#)]
38. Seu, R.; Biccari, D.; Orosei, R.; Lorenzoni, L.; Phillips, R.; Marinangeli, L.; Picardi, G.; Masdea, A.; Zampolini, E. SHARAD: The MRO 2005 shallow radar. *Planet. Space Sci.* **2004**, *52*, 157–166. [[CrossRef](#)]
39. Croci, R.; Seu, R.; Flamini, E.; Russo, E. The SHallow RADar (SHARAD) onboard the NASA MRO mission. *Proc. IEEE* **2011**, *99*, 794–807. [[CrossRef](#)]
40. Seu, R.; Phillips, R.J.; Biccari, D.; Orosei, R.; Masdea, A.; Picardi, G.; Safaeinili, A.; Campbell, B.A.; Plaut, J.J.; Marinangeli, L.; et al. SHARAD sounding radar on the Mars Reconnaissance Orbiter. *J. Geophys. Res. Planets* **2007**, *112*. [[CrossRef](#)]
41. Fois, F.; Mecozzi, R.; Iorio, M.; Calabrese, D.; Bombaci, O.; Catallo, C.; Croce, A.; Croci, R.; Guelfi, M.; Zampolini, E.; et al. Comparison between MARSIS & SHARAD results. In Proceedings of the 2007 IEEE International Geoscience and Remote Sensing Symposium, Barcelona, Spain, 23–28 July 2007; pp. 2134–2139.
42. Grima, C.; Kofman, W.; Mouginit, J.; Phillips, R.J.; Hérique, A.; Biccari, D.; Seu, R.; Cutigni, M. North polar deposits of Mars: Extreme purity of the water ice. *Geophys. Res. Lett.* **2009**, *36*. [[CrossRef](#)]
43. Selvens, M.; Aharonson, O.; Plaut, J.; Safaeinili, A. Structure of the basal unit of the north polar Plateau of Mars, from MARSIS. In Proceedings of the 2009 IEEE Radar Conference, Pasadena, CA, USA, 4–8 May 2009; pp. 1–3.
44. Smith, I.B.; Holt, J.W. Spiral trough diversity on the north pole of Mars, as seen by Shallow Radar (SHARAD). *J. Geophys. Res. Planets* **2015**, *120*, 362–387. [[CrossRef](#)]
45. Carter, L.M.; Campbell, B.A.; Watters, T.R.; Phillips, R.J.; Putzig, N.E.; Safaeinili, A.; Plaut, J.J.; Okubo, C.H.; Egan, A.F.; Seu, R.; et al. Shallow radar (SHARAD) sounding observations of the Medusae Fossae Formation, Mars. *Icarus* **2009**, *199*, 295–302. [[CrossRef](#)]
46. Simon, M.N.; Carter, L.M.; Campbell, B.A.; Phillips, R.J.; Mattei, S. Studies of lava flows in the Tharsis region of Mars using SHARAD. *J. Geophys. Res. Planets* **2014**, *119*, 2291–2299. [[CrossRef](#)]
47. Stuurman, C.; Osinski, G.; Holt, J.; Levy, J.; Brothers, T.; Kerrigan, M.; Campbell, B. SHARAD detection and characterization of subsurface water ice deposits in Utopia Planitia, Mars. *Geophys. Res. Lett.* **2016**, *43*, 9484–9491. [[CrossRef](#)]
48. Xiong, S.; Muller, J.P.; Tao, Y.; Ding, C.; Zhang, B.; Li, Q. Combination of MRO SHARAD and deep-learning-based DTM to search for subsurface features in Oxia Planum, Mars. *Astron. Astrophys.* **2023**, *676*, 13. [[CrossRef](#)]

49. Spagnuolo, M.; Grings, F.; Perna, P.; Franco, M.; Karszenbaum, H.; Ramos, V. Multilayer simulations for accurate geological interpretations of SHARAD radargrams. *Planet. Space Sci.* **2011**, *59*, 1222–1230. [[CrossRef](#)]
50. Restano, M.; Mastrogiuseppe, M.; Masdea, A.; Picardi, G.; Seu, R. Shallow Radar (SHARAD) investigations over Sinus Meridiani. In Proceedings of the 2012 IEEE International Geoscience and Remote Sensing Symposium, Munich, Germany, 22–27 July 2012; pp. 3206–3209.
51. Campbell, B.A.; Morgan, G.A. Fine-scale layering of Mars polar deposits and signatures of ice content in nonpolar material from multiband SHARAD data processing. *Geophys. Res. Lett.* **2018**, *45*, 1759–1766. [[CrossRef](#)]
52. Xiong, S.; Tao, Y.; Persaud, D.M.; Campbell, J.D.; Putri, A.R.D.; Muller, J.P. Subsurface reflectors detected by SHARAD reveal stratigraphy and buried channels over central Elysium Planitia, Mars. *Earth Space Sci.* **2021**, *8*, e2019EA000968. [[CrossRef](#)]
53. Zou, Y.; Zhu, Y.; Bai, Y.; Wang, L.; Jia, Y.; Shen, W.; Fan, Y.; Liu, Y.; Wang, C.; Zhang, A.; et al. Scientific objectives and payloads of Tianwen-1, China's first Mars exploration mission. *Adv. Space Res.* **2021**, *67*, 812–823. [[CrossRef](#)]
54. Hong, T.; Su, Y.; Dai, S.; Zhang, Z.; Du, W.; Liu, C.; Liu, S.; Wang, R.; Ding, C.; Li, C. An Improved Method of Surface Clutter Simulation Based on Orbiting Radar in Tianwen-1 Mars Exploration. *Radio Sci.* **2022**, *57*, e2022RS007491. [[CrossRef](#)]
55. Cartacci, M.; Amata, E.; Cicchetti, A.; Noschese, R.; Giuppi, S.; Langlais, B.; Frigeri, A.; Orosei, R.; Picardi, G. Mars ionosphere total electron content analysis from MARSIS subsurface data. *Icarus* **2013**, *223*, 423–437. [[CrossRef](#)]
56. Ilyushin, Y.A.; Kunitsyn, V. Methods for correcting ionosphere distortions of orbital ground-penetrating radar signals. *J. Commun. Technol. Electron. C/C Radiotekhnika I Elektron.* **2004**, *49*, 154–165.
57. Mouginot, J.; Kofman, W.; Safaeinili, A.; Hérique, A. Correction of the ionospheric distortion on the MARSIS surface sounding echoes. *Planet. Space Sci.* **2008**, *56*, 917–926. [[CrossRef](#)]
58. Safaeinili, A.; Kofman, W.; Nouvel, J.; Herique, A.; Jordan, R. Impact of Mars ionosphere on orbital radar sounder operation and data processing. *Planet. Space Sci.* **2003**, *51*, 505–515. [[CrossRef](#)]
59. Zhang, Z.; Nielsen, E.; Plaut, J.J.; Orosei, R.; Picardi, G. Ionospheric corrections of MARSIS subsurface sounding signals with filters including collision frequency. *Planet. Space Sci.* **2009**, *57*, 393–403. [[CrossRef](#)]
60. Alberti, G.; Dinardo, S.; Mattei, S.; Papa, C.; Santovito, M. SHARAD radar signal processing technique. In Proceedings of the 2007 4th International Workshop on, Advanced Ground Penetrating Radar, Naples, Italy, 27–29 June 2007; pp. 261–264.
61. Nouvel, J.F.; Herique, A.; Kofman, W.; Safaeinili, A. Radar signal simulation: Surface modeling with the facet method. *Radio Sci.* **2004**, *39*, 1–17. [[CrossRef](#)]
62. Herique, A.; Kofman, W.; Mouginot, J.; Eyraud, C.; Nouvel, J.F.; Safaeinili, A. Surface echo reduction by clutter simulation, Application to the Marsis data. In Proceedings of the 7th European Conference on Synthetic Aperture Radar, Friedrichshafen, Germany, 2–5 June 2008; pp. 1–4.
63. Restano, M.; Seu, R.; Picardi, G. A phase-gradient-autofocus algorithm for the recovery of marsis subsurface data. *IEEE Geosci. Remote Sens. Lett.* **2016**, *13*, 806–810. [[CrossRef](#)]
64. Withers, P. Attenuation of radio signals by the ionosphere of Mars: Theoretical development and application to MARSIS observations. *Radio Sci.* **2011**, *46*, 1–16. [[CrossRef](#)]
65. Jordan, R.; Picardi, G.; Plaut, J.; Wheeler, K.; Kirchner, D.; Safaeinili, A.; Johnson, W.; Seu, R.; Calabrese, D.; Zampolini, E.; et al. The Mars express MARSIS sounder instrument. *Planet. Space Sci.* **2009**, *57*, 1975–1986. [[CrossRef](#)]
66. Restano, M.; Masdea, A.; Picardi, G.; Seu, R. Weighting network influence on the geometric term correction in MARSIS data inversion. In Proceedings of the 2012 13th International Radar Symposium, Warsaw, Poland, 23–25 May 2012; pp. 213–217.
67. Ulaby, F.T.; Long, D.G.; Blackwell, W.J.; Elachi, C.; Fung, A.K.; Ruf, C.; Sarabandi, K.; Zebker, H.A.; Van Zyl, J. *Microwave Radar and Radiometric Remote Sensing*; University of Michigan Press: Ann Arbor, MI, USA, 2014; Volume 4.
68. Lauro, S.E.; Soldovieri, F.; Orosei, R.; Cicchetti, A.; Cartacci, M.; Mattei, E.; Cosciotti, B.; Di Paolo, F.; Noschese, R.; Pettinelli, E. Liquid water detection under the south polar layered deposits of Mars—A probabilistic inversion approach. *Remote Sens.* **2019**, *11*, 2445. [[CrossRef](#)]
69. Oswald, G.; Gogineni, S. Recovery of subglacial water extent from Greenland radar survey data. *J. Glaciol.* **2008**, *54*, 94–106. [[CrossRef](#)]
70. Zuber, M.T.; Phillips, R.J.; Andrews-Hanna, J.C.; Asmar, S.W.; Konopliv, A.S.; Lemoine, F.G.; Plaut, J.J.; Smith, D.E.; Smrekar, S.E. Density of Mars' south polar layered deposits. *Science* **2007**, *317*, 1718–1719. [[CrossRef](#)]
71. Maidique, M.; Von Hippel, A.; Westphal, W. Transfer of Protons through “Pure” Ice Ih Single Crystals. III. Extrinsic versus Intrinsic Polarization; Surface versus Volume Conduction. *J. Chem. Phys.* **1971**, *54*, 150–160. [[CrossRef](#)]
72. Pettinelli, E.; Cosciotti, B.; Di Paolo, F.; Lauro, S.E.; Mattei, E.; Orosei, R.; Vannaroni, G. Dielectric properties of Jovian satellite ice analogs for subsurface radar exploration: A review. *Rev. Geophys.* **2015**, *53*, 593–641. [[CrossRef](#)]
73. Kawada, S. Dielectric anisotropy in ice Ih. *J. Phys. Soc. Jpn.* **1978**, *44*, 1881–1886. [[CrossRef](#)]
74. Sihvola, A.H. *Electromagnetic Mixing Formulas and Applications*; Number 47; IET: Stevenage, UK, 1999.
75. Nerozzi, S.; Holt, J. Buried ice and sand caps at the north pole of Mars: Revealing a record of climate change in the cavi unit with SHARAD. *Geophys. Res. Lett.* **2019**, *46*, 7278–7286. [[CrossRef](#)]
76. Putzig, N.E.; Phillips, R.J.; Campbell, B.A.; Mellon, M.T.; Holt, J.W.; Brothers, T.C. SHARAD soundings and surface roughness at past, present, and proposed landing sites on Mars: Reflections at Phoenix may be attributable to deep ground ice. *J. Geophys. Res. Planets* **2014**, *119*, 1936–1949. [[CrossRef](#)]

77. Sori, M.M.; Bramson, A.M. Water on Mars, with a grain of salt: Local heat anomalies are required for basal melting of ice at the south pole today. *Geophys. Res. Lett.* **2019**, *46*, 1222–1231. [CrossRef]
78. Parro, L.M.; Jiménez-Díaz, A.; Mansilla, F.; Ruiz, J. Present-day heat flow model of Mars. *Sci. Rep.* **2017**, *7*, 45629. [CrossRef] [PubMed]
79. Plesa, A.C.; Padovan, S.; Tosi, N.; Breuer, D.; Grott, M.; Wieczorek, M.; Spohn, T.; Smrekar, S.; Banerdt, W. The thermal state and interior structure of Mars. *Geophys. Res. Lett.* **2018**, *45*, 12–198. [CrossRef]
80. Ruiz, J.; López, V.; Dohm, J.M. The present-day thermal state of Mars. *Icarus* **2010**, *207*, 631–637. [CrossRef]
81. Lauro, S.E.; Pettinelli, E.; Caprarelli, G.; Baniamerian, J.; Mattei, E.; Cosciotti, B.; Stillman, D.E.; Primm, K.M.; Soldovieri, F.; Orosei, R. Using MARSIS signal attenuation to assess the presence of South Polar Layered Deposit subglacial brines. *Nat. Commun.* **2022**, *13*, 5686. [CrossRef]
82. Orosei, R.; Caprarelli, G.; Lauro, S.; Pettinelli, E.; Cartacci, M.; Cicchetti, A.; Cosciotti, B.; De Lorenzis, A.; De Nunzio, G.; Mattei, E.; et al. Numerical simulations of radar echoes rule out basal CO₂ ice deposits at Ultimi Scopuli, Mars. *Icarus* **2022**, *386*, 115163. [CrossRef]
83. Lauro, S.E.; Pettinelli, E.; Caprarelli, G.; Guallini, L.; Rossi, A.P.; Mattei, E.; Cosciotti, B.; Cicchetti, A.; Soldovieri, F.; Cartacci, M.; et al. Reply to: Explaining bright radar reflections below the south pole of Mars without liquid water. *Nat. Astron.* **2023**, *7*, 259–261. [CrossRef]
84. Pettinelli, E.; Vannaroni, G.; Cereti, A.; Paolucci, F.; Della Monica, G.; Storini, M.; Bella, F. Frequency and time domain permittivity measurements on solid CO₂ and solid CO₂–soil mixtures as Martian soil simulants. *J. Geophys. Res. Planets* **2003**, *108*. [CrossRef]
85. Jones, Eriita G. Shallow transient liquid water environments on present-day Mars, and their implications for life. *Acta Astronautica*. **2018**, *146*, 144–150. [CrossRef]
86. Murray, A.; Fritsen, C.; Kenig, F.; McKay, C.; McNight, D.; Cawley, K.; Doran, P. Life in the ice cover and underlying cold brines of Lake Vida, Antarctica. *Geochim. Cosmochim. Acta Suppl.* **2009**, *73*, A922.
87. Murray, A.E.; Kenig, F.; Fritsen, C.H.; McKay, C.P.; Cawley, K.M.; Edwards, R.; Kuhn, E.; McKnight, D.M.; Ostrom, N.E.; Peng, V.; et al. Microbial life at -13 C in the brine of an ice-sealed Antarctic lake. *Proc. Natl. Acad. Sci. USA* **2012**, *109*, 20626–20631. [CrossRef]
88. Mondino, L.J.; Asao, M.; Madigan, M.T. Cold-active halophilic bacteria from the ice-sealed Lake Vida, Antarctica. *Arch. Microbiol.* **2009**, *191*, 785–790. [CrossRef] [PubMed]
89. Heinz, J.; Krahn, T.; Schulze-Makuch, D. A new record for microbial perchlorate tolerance: Fungal growth in NaClO₄ brines and its implications for putative life on Mars. *Life* **2020**, *10*, 53. [CrossRef]
90. Reid, I.; Sparks, W.; Lubow, S.; McGrath, M.; Livio, M.; Valenti, J.; Sowers, K.; Shukla, H.; MacAuley, S.; Miller, T.; et al. Terrestrial models for extraterrestrial life: Methanogens and halophiles at Martian temperatures. *Int. J. Astrobiol.* **2006**, *5*, 89–97. [CrossRef]
91. DasSarma, P.; Laye, V.; Harvey, J.; Reid, C.; Shultz, J.; Yarborough, A.; Lamb, A.; Koske-Phillips, A.; Herbst, A.; Molina, F.; et al. Survival of halophilic Archaea in Earth's cold stratosphere. *Int. J. Astrobiol.* **2017**, *16*, 321–327. [CrossRef]
92. Landis, G.A. Martian water: Are there extant halobacteria on Mars? *Astrobiology* **2001**, *1*, 161–164. [CrossRef]
93. Landis, G.A. Searching for life: The case for Halobacteria on Mars. *AIP Conf. Proc.* **2001**, *552*, 25–28.
94. DasSarma, S.; Arora, P. Halophiles. *Encycl. Life Sci.* **2001**. [CrossRef]
95. DasSarma, S. Extreme halophiles are models for astrobiology. *Microbe-Am. Soc. Microbiol.* **2006**, *1*, 120. [CrossRef]
96. Franzmann, P.; Stackebrandt, E.; Sanderson, K.; Volkman, J.; Cameron, D.; Stevenson, P.; McMeekin, T.; Burton, H. Halobacterium lacusprofundi sp. nov., a halophilic bacterium isolated from Deep Lake, Antarctica. *Syst. Appl. Microbiol.* **1988**, *11*, 20–27. [CrossRef]
97. Aerts, J.W.; Riedo, A.; Melton, D.J.; Martini, S.; Flahaut, J.; Meierhenrich, U.J.; Meinert, C.; Myrgorodska, I.; Lindner, R.; Ehrenfreund, P. Biosignature analysis of Mars soil analogs from the Atacama Desert: Challenges and implications for future missions to Mars. *Astrobiology* **2020**, *20*, 766–784. [CrossRef] [PubMed]
98. Xu, L.; Li, H.; Pei, Z.; Zou, Y.; Wang, C. A Brief Introduction to the International Lunar Research Station Program and the Interstellar Express Mission. *Chin. J. Space Sci.* **2022**, *42*, 511–513. [CrossRef]
99. Sun, Z. Prospects for Mars Exploration and Sample Return. Available online: <https://www.koushare.com/video/videodetail/41321> (accessed on 6 June 2022).
100. Xiao, L. Evolution of the Geological Environment and Exploration for Life on Mars. *J. Earth Sci.* **2023**, *34*, 1626–1628. [CrossRef]
101. Fairén, A.G.; Davila, A.F.; Lim, D.; Bramall, N.; Bonaccorsi, R.; Zavaleta, J.; Uceda, E.R.; Stoker, C.; Wierzchos, J.; Dohm, J.M.; et al. Astrobiology through the ages of Mars: The study of terrestrial analogues to understand the habitability of Mars. *Astrobiology* **2010**, *10*, 821–843. [CrossRef]
102. Horneck, G.; Baumstark-Khan, C. *Astrobiology: The Quest for the Conditions of Life*; Springer Science & Business Media: Berlin/Heidelberg, Germany, 2012.
103. Nagy, B.; Kovács, J.; Ignécz, Á.; Beleznai, S.; Mari, L.; Kereszturi, Á.; Szalai, Z. The thermal behavior of ice-bearing ground: The highest cold, dry desert on Earth as an analog for conditions on Mars, at Ojos del Salado, Puna De Atacama-Altiplano region. *Astrobiology* **2020**, *20*, 701–722. [CrossRef]
104. Hallsworth, J.E.; Mancinelli, R.L.; Conley, C.A.; Dallas, T.D.; Rinaldi, T.; Davila, A.F.; Benison, K.C.; Rapoport, A.; Cavalazzi, B.; Selbmann, L.; et al. Astrobiology of life on Earth. *Environ. Microbiol.* **2021**, *23*, 3335–3344. [CrossRef]

105. Kurokawa, H.; Sato, M.; Ushioda, M.; Matsuyama, T.; Moriwaki, R.; Dohm, J.M.; Usui, T. Evolution of water reservoirs on Mars: Constraints from hydrogen isotopes in martian meteorites. *Earth Planet. Sci. Lett.* **2014**, *394*, 179–185. [[CrossRef](#)]
106. Rotelli, L.; Trigo-Rodríguez, J.M.; Moyano-Camero, C.E.; Carota, E.; Botta, L.; Di Mauro, E.; Saladino, R. The key role of meteorites in the formation of relevant prebiotic molecules in a formamide/water environment. *Sci. Rep.* **2016**, *6*, 38888. [[CrossRef](#)]
107. Cronin, J.R.; Pizzarello, S.; Cruikshank, D.P. Organic matter in carbonaceous chondrites, planetary satellites, asteroids and comets. *Meteorites Early Sol. Syst.* **1988**, 819–857.
108. Nyquist, L.; Bogard, D.; Shih, C.Y.; Greshake, A.; Stöffler, D.; Eugster, O. Ages and geologic histories of Martian meteorites. In Proceedings of the Chronology and Evolution of Mars: Proceedings of an ISSI Workshop, Bern, Switzerland, 10–14 April 2000; Springer: Berlin/Heidelberg, Germany, 2001; pp. 105–164.
109. Jull, A.; Eastoe, C.; Xue, S.; Herzog, G. Isotopic composition of carbonates in the SNC meteorites Allan Hills 84001 and Nakhla. *Meteoritics* **1995**, *30*, 311–318. [[CrossRef](#)]
110. Moyano-Camero, C.E.; Trigo-Rodríguez, J.M.; Benito, M.I.; Alonso-Azcárate, J.; Lee, M.R.; Mestres, N.; Martínez-Jiménez, M.; Martín-Torres, F.J.; Fraxedas, J. Petrographic and geochemical evidence for multiphase formation of carbonates in the Martian orthopyroxenite Allan Hills 84001. *Meteorit. Planet. Sci.* **2017**, *52*, 1030–1047. [[CrossRef](#)]
111. Velbel, M.A. Aqueous corrosion of olivine in the Mars meteorite Miller Range (MIL) 03346 during Antarctic weathering: Implications for water on Mars. *Geochim. Cosmochim. Acta* **2016**, *180*, 126–145. [[CrossRef](#)]
112. Trigo-Rodríguez, J.M.; Trišić, J. What can be learned from Allan Hills 84001 carbonate globules about aqueous alteration processes in the Martian crust? In Proceedings of the European Planetary Science Congress, 2021, Online, 13–24 September 2021; EPSC2021-803. [[CrossRef](#)]
113. Muirhead, B.K.; Nicholas, A.; Umland, J. Mars sample return mission concept status. In Proceedings of the 2020 IEEE Aerospace Conference, Big Sky, Montana, 7–14 March 2020; pp. 1–8.
114. Muirhead, B.K.; Nicholas, A.K.; Umland, J.; Sutherland, O.; Vijendran, S. Mars Sample Return Campaign Concept Status. *Acta Astronaut.* **2020**, *176*, 131–138. [[CrossRef](#)]

Disclaimer/Publisher’s Note: The statements, opinions and data contained in all publications are solely those of the individual author(s) and contributor(s) and not of MDPI and/or the editor(s). MDPI and/or the editor(s) disclaim responsibility for any injury to people or property resulting from any ideas, methods, instructions or products referred to in the content.